Methane + Propane Structure II Hydrate Formation Kinetics

Ramesh A. Kini,[†] Steven F. Dec, and E. Dendy Sloan, Jr.*

Center for Hydrate Research, Colorado School of Mines, Golden, Colorado 80401

Received: April 21, 2004; In Final Form: July 15, 2004

The growth rates of methane (CH_4) + propane (C_3H_8) structure II (sII) hydrates were measured via ^{13}C NMR in a custom-built nonspinning probe. The $CH_4 + C_3H_8$ hydrate surface reaction growth data suggested that the large cages occupied by C_3H_8 formed twice as fast as small cages filled with CH_4, although there were half as many large $5^{12}6^4$ cages as small 5^{12} cages in a sII unit cell. Growth rates were measured at 269 K as a function of ice particle size ranging between 150 and 1180 μm, and vapor pressure in the range 0.34−0.84 MPa. A hypothesis based on low occupancy of sII small cages was presented to explain faster growth of large cages. A simple surface reaction model, which related growth rate to pressure and particle size, was developed.

1. Introduction

Natural gas hydrates, the inclusion compounds of natural gas and water, form in oil and gas producing pipelines, when the pipeline pressure (*P*) and temperature (*T*) lie within the hydrate stability envelope. Without proper precautions, hydrates can eventually block pipelines resulting in production losses. Hydrate growth measurements can be used to better quantify hydrate formation rates, and hence, to improve hydrate plug prevention strategies.

Because natural gas contains propane and higher hydrocarbons,[1] hydrates that form in gas producing pipelines are usually structure II (sII). To prevent hydrate formation in a pipeline, the pipeline fluid pressure and temperature are maintained outside the hydrate stability region with the injection of inhibitors. Nonetheless, hydrates might form in the system due to operational or technical failures. Hydrate particles grow and agglomerate to eventually plug the pipeline. Hydrate growth measurements can be used to estimate hydrate plug formation time.

The current understanding of hydrate growth kinetics is minimal compared to the state-of-the-art knowledge of hydrate structure and thermodynamics.[2] Until spectroscopic techniques became available, most researchers measured the rate of consumption of gas during hydrate formation by monitoring the system pressure change, thereby indirectly determining hydrate growth rate via gas inclusion. The results from such experiments were difficult to reproduce and hence, the kinetic models generated were specific to the experiments.[3] These kinetics measurements were confounded by heat and mass transfer limitations. Nevertheless, many natural gas hydrate formation mechanisms were developed using such data but were not further validated using data from other research groups.[4] Further references on kinetic studies can be found in the reviews by Sloan[2] and Englezos.[5]

Pietrass et al.[6] used hyperpolarized-^{129}Xe NMR spectroscopy to directly measure structure I (sI) Xe hydrate formation from ice. On the basis of similar experiments, Moudrakovski et al.[7] suggested that NMR measurements do not have limitations from transport phenomena. Fleyfel et al. investigated $CH_4 + C_3H_8$ hydrate formation from water via ^{13}C NMR.[8] Other techniques such as Raman spectroscopy and neutron diffraction have recently been used to measure sI methane hydrate kinetics.[9,10]

The NMR spectroscopic technique differs from the conventional nonspectroscopic methods in that NMR directly measures change in the number of guest-occupied cages during hydrate formation. Gas mixtures of CH_4 and C_3H_8 are predicted to form sII hydrates with as little as 1% propane,[2] and hence this binary gas mixture was used in this study. In this work, we report the rate of $CH_4 + C_3H_8$ sII hydrate formation from ice using ^{13}C NMR spectroscopy. These are the first kinetic NMR measurements of binary natural gas hydrate formation from ice.

2. Experimental Section

A custom-built probe capable of external control of sample pressure and in situ formation of hydrates was used to make the NMR measurements reported in this study. The probe had two channels that could simultaneously irradiate the sample at two resonance frequencies, e.g., ^1H and ^{13}C. The probe head is shown in Figure 1 with the sample cell inserted in the radio frequency (RF) coil. The sample cell was kept cold by passing temperature-controlled N_2 gas in a temperature chamber housing the coil-sample cell assembly. The probe had a temperature range from 153 to 373 K.

Initially the sample cell was packed with powdered ice, which was prepared by grinding ice with a mortar and pestle. The ice particles of a particular size range were separated from this powder using LN_2-cooled metal sieves. The ice-filled sample cell was inserted in the NMR coil and cooled to about 253 K with a stream of temperature controlled nitrogen gas. The sample cell was evacuated, warmed to 269 ± 0.5 K, and charged with the hydrate former gas via a $^1/_{16}$ in. stainless steel tube, attached to the sample cell as shown in Figure 1. The NMR data acquisition was immediately started. During hydrate formation, the gas mixture was pressurized by a piston pump, and the sample cell pressure was measured with a Heise gauge. Upon contact with ice, the gas formed hydrates while the hydrate NMR spectra were collected.

In these experiments, the feed gas was a mixture of enriched methane ($^{13}CH_4$) and enriched propane ($^{13}CH_3-CH_3-CH_3$)

* Corresponding author. Phone: 303-273-3723. Fax: 303-273-3730. E-mail: esloan@mines.edu.

[†] Current address: ChevronTexaco, 2811 Hayes Road, Houston, TX 77082.

10.1021/jp040301l CCC: $27.50
Published on Web 10/07/2004

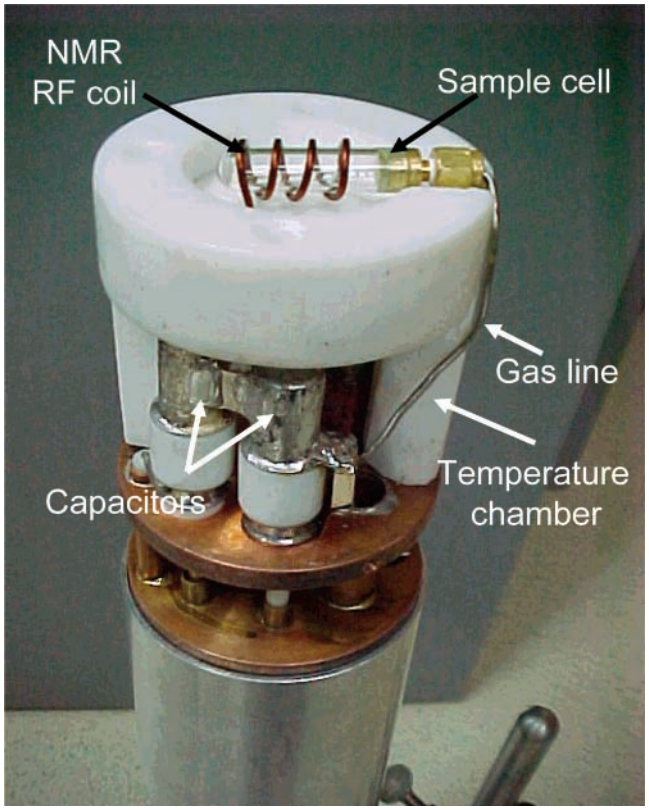

Figure 1. Probe-head picture showing (1) NMR radio frequency (RF) coil, (2) sample cell, (3) gas line, (4) temperature chamber, and (5) capacitors (electronic circuit components).

obtained from Isotec Inc. Both gases were 99 atom % ^{13}C pure (minimum) and no impurity could be detected chromatographically. All gas mixtures were made gravimetrically and were mixed by thermal agitation.

3. NMR Experiments

All NMR spectra were recorded using a Chemagnetics CMX Infinity 400 spectrometer operating at 100.6 MHz for ^{13}C. All ^{13}C NMR spectra were recorded with single-pulse excitation (90° pulse of 7 μs), proton decoupling field strength of 35.7 kHz, and a relaxation delay of 10 s. A relaxation delay of 10 s was sufficient to obtain fully relaxed spectra so that quantitative relative intensities were obtained. Spectra were averaged over 64 scans. The methyl carbon resonance peak of hexamethylbenzene (HMB), assigned a chemical shift of 17.36 ppm, was used as an external chemical shift reference.[11] Methanol was used to calibrate the sample temperature using a correlation relating ^1H chemical shift difference between the methyl and the hydroxyl groups of methanol and the absolute sample temperature.[12]

4. Results

4.1. Time Development of $CH_4 + C_3H_8$ sII Spectrum. Figure 2 shows a ^{13}C NMR spectrum of $CH_4 + C_3H_8$ sII hydrate obtained 0.69 MPa and 270 K. Propane was present in large $5^{12}6^4$ cages of sII hydrate and in the vapor, and methane was present in small 5^{12} cages of sII hydrate as well as in vapor. Any propane in the sII small cages, or methane in the sII large cages was not detected due to low spectral resolution. However, the occupancy of methane in the large cages of $CH_4 + C_3H_8$ sII hydrates was shown to be only 14% of the total amount of methane in the hydrate.[13] Propane molecules with a van der

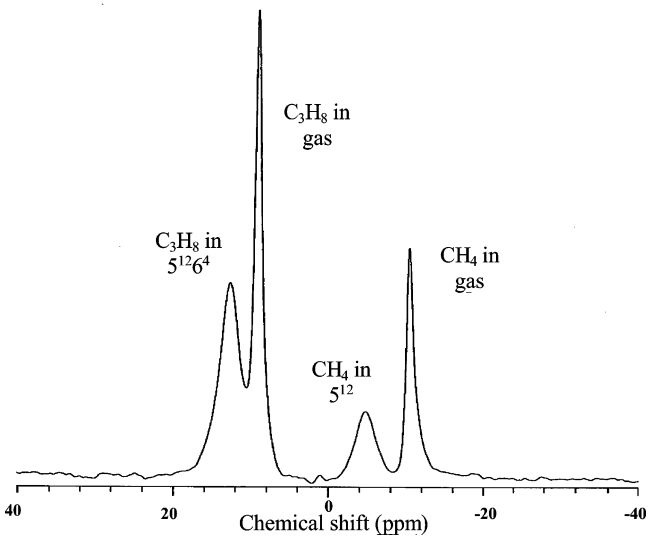

Figure 2. Nonspinning ^{13}C NMR spectrum of $CH_4 + C_3H_8$ sII hydrate at 0.69 MPa and 270 K.

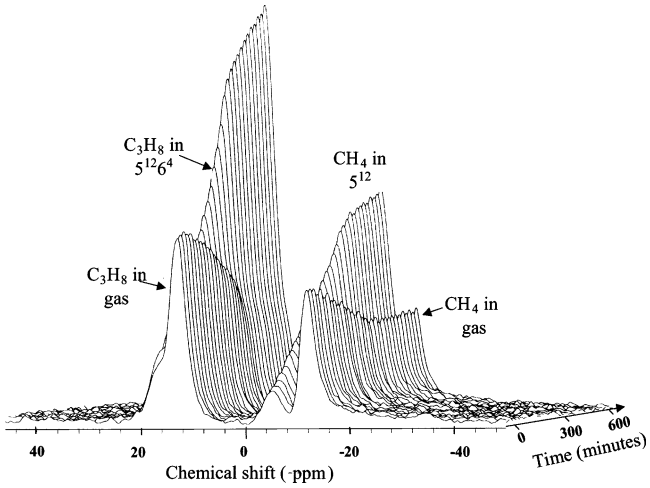

Figure 3. Time variant plot of ^{13}C NMR spectra of $CH_4 + C_3H_8$ sII hydrate formation from ice at 270 K.

Waals radius of 3.14 Å are probably too large to fit in a sII 5^{12} cage with an average free radius of 2.5 Å. The magic-angle-spinning spectrum of $CH_4 + C_3H_8$ hydrate formed with a similar feed composition[13] suggested that the $CH_4 + C_3H_8$ gas mixture formed only sII hydrates without simultaneous formation of sI and sII. The chemical shifts for methane and propane in the hydrate phase shown in Figure 2 were indicative of sII hydrate. This interpretation was based on the comparison between the chemical shifts in Figure 2 and those measured by Ripmeester and Ratcliffe.[13] In this work, each spectrum was time averaged over 640 s. Peak areas were deconvoluted using SPINSIGHT curve fitting software from Varian, Inc.

A typical time plot of $CH_4 + C_3H_8$ hydrate formation from ice is shown in Figure 3. The spectrum acquisition was started after the gas mixture was delivered to the cell that contained fresh ice powder. The spectra were collected for periods as long as 10 h. The change in peak areas reflected the change in vapor and hydrate composition. Figure 3 shows gas was consumed as hydrates formed. The feed gas mixture was continually stripped of propane as the experiment progressed.

A similar change in vapor composition was observed by Uchida et al.[14] during their $CH_4 + C_3H_8$ sII hydrate formation experiment. In that study, gas chromatographic analysis of vapor showed that CH_4 and C_3H_8 were simultaneously consumed

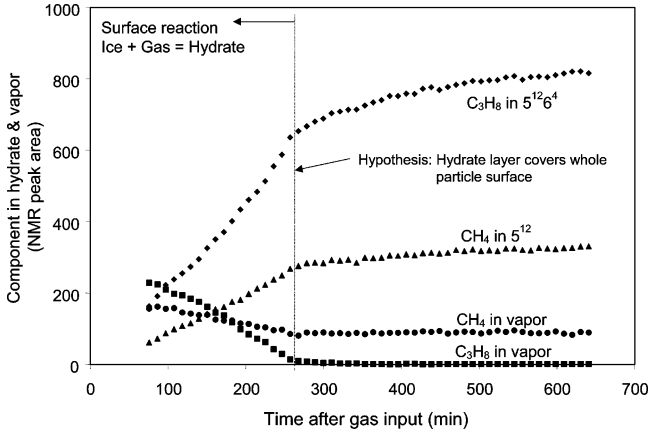

Figure 4. Typical relative change in CH_4 and C_3H_8 concentrations in hydrate and vapor phases (in terms of NMR peak areas) with time (in minutes) after gas charge.

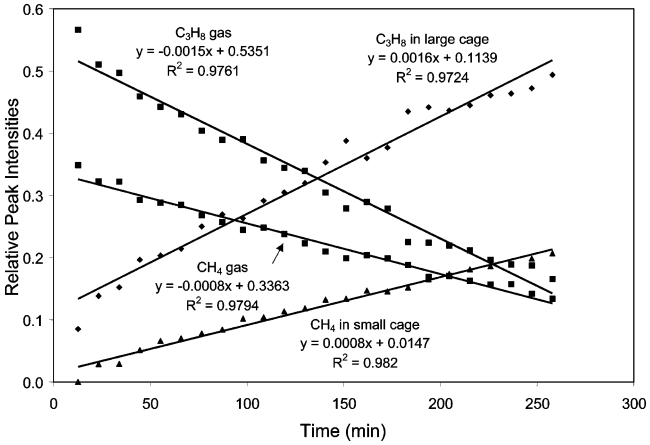

Figure 5. Hydrate and vapor compositions as a function of time in the surface reaction regime of hydrate formation with ice particle of 840 μm $< D <$ 1180 μm at 0.67 MPa and 269 $\pm$ 0.5 K. Peak areas are normalized by the sum of all peak areas and expressed as fractions. In the linear fit equations, x is time (min), y is the normalized peak area, and R is the correlation coefficient.

during hydrate formation. Propane was consumed at a higher rate as hydrates formed until C_3H_8 was completely consumed, leaving almost pure CH_4 in the vapor. Their subsequent CH_4 consumption from vapor yielded trace amounts of sI hydrates in the system.

The peak areas obtained from the spectra shown in Figure 3 are plotted as a function of time in Figure 4. Both hydrate and vapor curves had linear slopes until 260 min, after which they entered a slow growth regime. During linear growth, the methane and propane hydrate peak intensities increased linearly with time, as shown by the slope of hydrate peak areas. The methane and propane content in vapor decreased linearly as gas was consumed. The system pressure decreased due to gas consumption by only about 0.007 MPa (1 psia). The error in CH_4 and C_3H_8 gas peak areas increased from 1 to 3% and 2 to 3%, respectively, over the course of the experiment. Similarly, the error in CH_4 and C_3H_8 hydrate peak areas decreased from 9 to 2% and 5 to 1%, respectively. Two types of hydrate growths were typically observed in time plots such as Figure 4—a fast linear growth and a slower nonlinear growth.

4.2. Cage Growth Measurements. In Figure 4, the linear part of the growth curve was attributed to hydrate formation from a surface reaction between ice and gas. This hypothesis (see section 4.3) was based on the linear growth rate dependency on both the surface-to-volume ratio of ice particle and the partial pressure of gas. Because hydrates formed from fresh ice powder, abundant surface nucleation sites were initially available for reaction. The feed gas was in excess of the amount of ice in the sample, because the volume of the gas line was about 250 times larger than the sample cell volume. Hence, gas-phase mass transfer limitations to kinetics were assumed to be negligible.

Because hydrate formation is an exothermic process, the conversion of ice to hydrate results in the evolution of heat at the reaction sites. The heat generated during hydrate formation was, however, too small to affect kinetic measurements based on the following calculations. The temperature change due to this heat generation was calculated to be approximately 1.5 K to form a 1 μm thick hydrate layer on the surface of a 500 μm diameter ice particle. This temperature gradient was reduced by about 0.95 K due to heat consumption while ice was melted during hydrate formation (see Appendix A for calculations). Heat transfer limitations could therefore be neglected. As a result, the measured growth rates were considered due to kinetics of hydrate formation reaction, with neither heat nor mass transfer limitations.

The decreased slopes of nonlinear growth, which begin at 260 min in Figure 4, suggested a slower rate in both vapor and hydrate. This slower rate of hydrate formation was hypothesized to be due to the presence of a surface hydrate layer, which hindered the transport of methane and propane into the ice particle core for further reaction. The change in slope, or the transition from a fast growth to a slow growth regime, suggested that the surface reaction went to completion as the particle surface was completely covered with a hydrate layer. The time at which this sharp change occurred was referred to as "surface saturation time".

From the linear growth regime, the slopes of methane and propane concentration in hydrate and vapor were determined. The slope of the area under the peak due to methane in 5^{12} small cages versus time was proportional to the growth rate of 5^{12} cages occupied by methane. Similarly, the slope of the peak area due to propane in hydrate versus time was proportional to the growth rate of $5^{12}6^4$ cages occupied by propane. The slope of vapor peak areas was proportional to the rate at which the components were consumed from vapor phase. These slopes were measured for three different ice particle size ranges between 150 and 1180 μm and six different pressures between 0.34 and 0.84 MPa. The surface saturation time was also measured as a function of ice particle size and pressure. In the slow growth regime, the slopes of both hydrate and vapor peaks were small and the propane vapor peak intensity was too small to be determined accurately.

Hydrate formation rates during initial surface reaction suggested a growth mechanism for methane + propane sII hydrate. The initial linear parts of the hydrate growth and gas consumption curves are plotted in Figure 5. Table 1 summarizes the formation rate of $5^{12}6^4$ occupied by propane (G), corresponding average particle diameters (D) and pressures in these experiments. The formation rates of both $5^{12}6^4$ cages occupied by propane and 5^{12} cages occupied by methane are summarized in Table 2. The ratio of formation rates suggested that propane-occupied $5^{12}6^4$ cages formed twice as fast as methane-occupied 5^{12} cages.

Figure 5 and Table 2 show that both methane and propane were conserved in this system. The rate at which small and large hydrate cages were occupied is equal in magnitude but of opposite sign to the rate at which methane and propane gas were removed from the gas phase. In an experiment with the

TABLE 1: List of Experimental Parameters and Corresponding $5^{12}6^4$ Formation Rates

P_{TOTAL} (MPa)	$P_{PROPANE}$ (MPa)	av particle size (D, mm)	surface/volume ($1/D$)	formation rate of $5^{12}6^4$ occupied by C_3H_8 (G, molecules/min)
0.48	0.28	375	0.00267	0.0018
0.69	0.42	375	0.00267	0.0020
0.34	0.23	375	0.00267	0.0011
0.50	0.31	375	0.00267	0.0022
0.84	0.45	375	0.00267	0.0057
0.81	0.43	375	0.00267	0.0032
0.63	0.43	200	0.00500	0.0026
0.67	0.41	1010	0.00099	0.0016

TABLE 2: List of Formation Rates of Hydrate Cages and Consumption Rates of CH_4 and C_3H_8

$P_{PROPANE}$ (MPa)	$P_{METHANE}$ (MPa)	formation rate		consumption rate		ratio of formation rates $5^{12}6^4/5^{12}$
		C_3H_8 in $5^{12}6^4$	CH_4 in 5^{12}	C_3H_8 vapor	CH_4 vapor	
0.28	0.20	0.0018	0.0007	−0.0018	−0.0007	2.57
0.42	0.27	0.0020	0.0010	−0.0020	−0.0010	2.00
0.23	0.11	0.0011	0.0007	−0.0011	−0.0007	1.69
0.31	0.19	0.0022	0.0001	−0.0021	−0.0002	22.00
0.45	0.39	0.0057	0.0030	−0.0054	−0.0033	1.90
0.43	0.38	0.0032	0.0022	−0.0032	−0.0020	1.45
0.43	0.20	0.0026	0.0011	−0.0026	−0.0011	2.36
0.41	0.26	0.0016	0.0008	−0.0015	−0.0008	2.00

propane partial pressure of 0.31 MPa, the ratio of large to small cage growth rates was 22.00, which was an order of magnitude greater than the growth rate ratios in other experiments; this single abnormally high value was attributed to the error due to low signal-to-noise ratio in this case. Excluding this data point, the average ratio of large to small cage growth rates is 2.0 ± 0.4. Figure 1S (see Supporting Information) shows a plot of the ratio of large cage to small cage peak areas as function of time in the linear growth regime for the data shown in Figures 4 and 5. The ratio approaches a value corresponding to the equilibrium ratio for long times as might be expected. Studies using a wider range of $CH_4 + C_3H_8$ feed ratios should be performed before any special significance is attributed to the 2:1 ratio of growth rates observed in this work.

4.3. Surface Reaction Growth Model. In general, the irreversible reaction of a gas at a solid interface depends on (1) diffusion of the gas to the surface, (2) adsorption of the gas at the surface, and (3) chemical reaction to form the product. The rate of reaction for the case where products are formed each time a gas molecule strikes the solid interface is given by Gardiner[15]

$$R = kA_S P_G \tag{1}$$

R is the rate of reaction, k is the rate constant, A_S is the surface area per unit volume of the solid, and P_G is the partial pressure of the gas. Equation 1 indicates that R increases linearly with both A_S and P_G. The rate of reaction (vapor + ice → hydrate) is equal to the rate of surface hydrate formation.

The initial rate of reaction should be proportional to the total surface area.[16] The surface area can be normalized to the total volume because the sample cell volume (V_o) and ice filling procedure were approximately constant in all our experiments. Assuming a constant space filling ratio (α), the total volume of ice particles (V_T) remained constant in our experiments. The space filling ratio is the fraction of a sample filled by ice. The total volume of ice particles in a sample is

$$V_T = V_o\alpha = \text{a constant} \tag{2}$$

The total number of particles in a sample is

$$N = V_T(1/V) \tag{3}$$

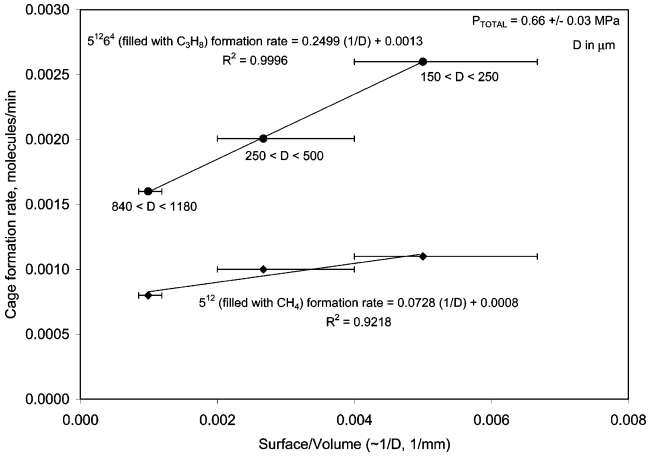

Figure 6. Reaction rates (rate of formation of $5^{12}6^4$ filled with C_3H_8 and that of 5^{12} filled with CH_4) increasing linearly with the particle surface-to-volume ratio.

where V is the volume of an ice particle. The total surface area of ice particles is

$$(S_T) = SN = SV_T/V = (S/V)V_T \tag{4}$$

where S is the surface area of a single ice particle.

Because V_T is constant, the total surface area is proportional to the surface-to-volume ratio. Therefore, the growth rate is linearly proportional to the total surface area of ice particles in a sample.

If the initial hydrate formation rate was a surface phenomenon, then eq 1 indicates that the rate of hydrate cage formation should vary linearly with both the surface area per unit volume (A_S) and the gas partial pressure. Figure 6 shows a plot of sII small and large cage formation rates as a function of A_S.

Figure 7 shows a plot of sII large cage formation rate as a function of propane partial pressure ($P_{propane}$). As indicated in Figures 6 and 7, the rate of sII large cage formation depended linearly on both A_S and $P_{propane}$, suggesting that the initial rate corresponded to a simple surface reaction. Similarly, Figure 8 showed that the rate at which CH_4 occupied the 5^{12} cages depended linearly on methane partial pressure ($P_{methane}$), also suggesting an initial surface reaction. The linear relation between

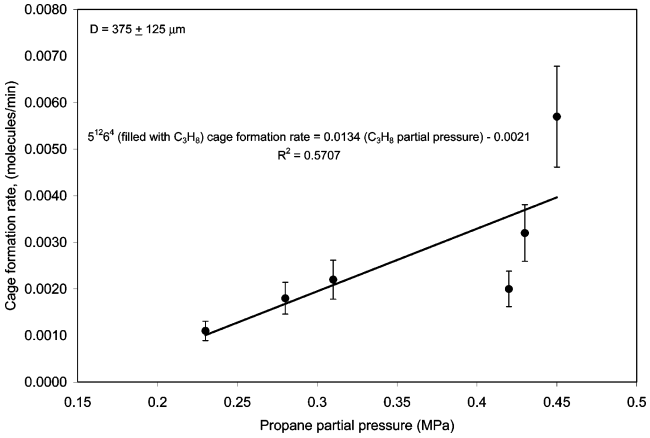

Figure 7. Effect of C_3H_8 partial pressure on $5^{12}6^4$ cage formation rate.

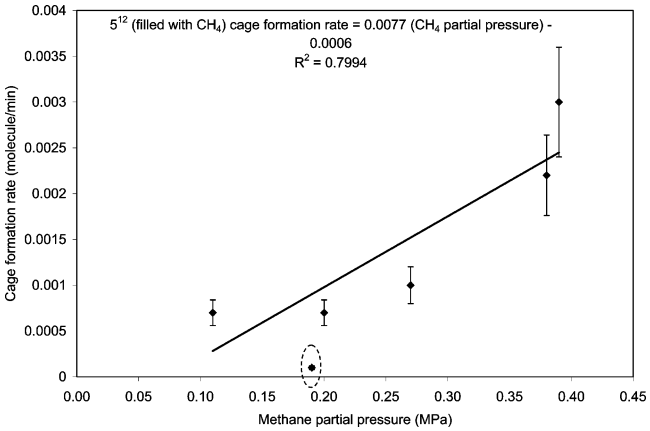

Figure 8. Effect of CH_4 partial pressure on 5^{12} cage formation rate. See text for explanation of encircled point.

cage formation rate and pressure is a first approximation because of a significant error (±20%) in the cage formation rate. The validity of a nonlinear relation should be tested by collecting more precise data at higher pressures and multiple temperatures. The datapoint marked with a dashed elipse in Figure 8 corresponded to an experiment with small methane 5^{12} cage peak areas, which could not be accurately measured. The partial pressures of methane and propane were measured at the start of the experiment.

The surface saturation time at which the linear growth ended, decreased linearly with the increasing average surface-to-volume ratio of ice particles, as shown in Figure 9. The error bars on the particle size accounted for the range of particle size used. The surface-to-volume ratio was inversely proportional to the particle diameter. As the particle diameter decreased, the surface area decreased, and hence the time required to saturate the particle surface with hydrate layer decreased.

If the relation between the surface saturation time and surface-to-volume ratio is extrapolated to small particles, a particle diameter of 120 μm (corresponding to $A_s = 1/D = 0.0083\ \mu m^{-1}$ when $T_s = 0$ min) yields a "zero" surface saturation time. Future experiments should include particles smaller than 120 μm to determine whether a slow growth region is observed.

As stated above, the growth was linear during surface reaction. At the surface saturation time, the surface reaction ended due to the lack of reaction sites on the surface. At this time, the hydrate layer completely covered the particle surface blocking the contact between ice and gas. Further growth was probably controlled by the diffusion of gas to the particle core through cracks and defects in the hydrate layer, and hence was

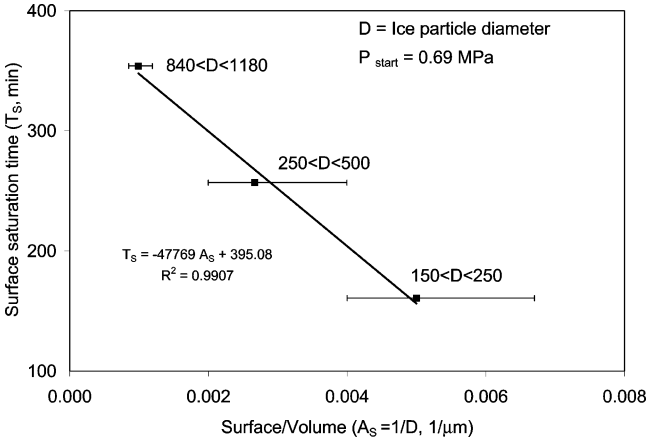

Figure 9. Surface saturation time as a linear function of surface-to-volume ratio.

slower. Because the amount of ice in the sample cell was not measured, we assumed that the ice particles initially occupied 75% of the sample cell. The amount of gas consumed during the surface reaction was used to calculate the total number of sII unit cells that constituted the hydrate layer. Assuming that the unit cells uniformly covered the particle surface in layers, the hydrate layer was estimated to be in the range of 0.1−30 μm.

5. $CH_4 + C_3H_8$ Structure II Hydrate Formation Mechanism

NMR and Raman spectroscopy have previously been used to study hydrate cage formation rates in xenon (from xenon gas and ice)[6] and methane (from methane gas and liquid water) sI hydrates,[9] respectively. For both sI hydrates, the small cages were observed to form faster at an early stage, although there are 3 times more large cages than small cages in the sI hydrate unit cell. In contrast, NMR measurements on $CH_4 + C_3H_8$ sII hydrate in this work suggested that large cages filled with C_3H_8 form twice as fast as small cages occupied by CH_4, although there are half as many large cages as small cages in a structure II unit cell. This result differs from that of Fleyfel and co-workers[8] who concluded that the small cage filled more rapidly on the basis of ^{13}C NMR studies of the formation of sII hydrate from $CH_4 + C_3H_8$ gas mixtures and liquid water. The discrepancy between these two results may be that ice is used in our study or that the gas feed used in the work of Fleyfel and co-workers had a much higher concentration (96%) of CH_4 than that used in our study. Additional work with a wider range of CH_4 and C_3H_8 gas compositions are needed to explicitly resolve this issue.

5.1. $CH_4 + C_3H_8$ sII Formation with a Small 5^{12} Occupancy. One hypothesis that was advanced as an explanation for sI formation kinetics with methane is that it is kinetically more favorable to rearrange the 20 water molecules of the small 5^{12} cage in sI hydrate relative to the 24 water molecules of the large $5^{12}6^2$ cage.[17] Although this hypothesis seemed intuitively reasonable, the current work suggested that, at least in sII, the hydrate cage formation rate was controlled by other factors. For sII hydrates, the faster forming large $5^{12}6^4$ cage was made of 28 water molecules whereas the small 5^{12} cage had only 20 water molecules. The slow growth regime may be diffusion-limited but cannot be analyzed using a shrinking core model[18] because we measured only the number of hydrate cages occupied by CH_4 and C_3H_8 and not the total amount of hydrate present.

We provide the following alternative hypothesis to explain hydrate formation kinetics in both sI and sII. The ratio of guest diameter to cage diameter (*S*) is a rough measure of cage stability. A $5^{12}6^4$ cage with a propane molecule is more stable, with *S* equal to 0.943, than a 5^{12} cage occupied by methane with an *S* of 0.855. Due to higher stability, the large cages with propane may form more readily than small cages with methane. Therefore, the small cage formation rate limits the overall sII hydrate growth rate in $CH_4 + C_3H_8$ sII hydrate. This is in contrast with the earlier pure methane sI kinetic observation that the formation of large cages, which form slower than small cages, limit the rate of sI formation.[6,9] The *S* ratios for methane sI hydrate are 0.855 for the small 5^{12} cage and 0.744 for the large $5^{12}6^4$ cage and for xenon sI hydrate the *S* values are 0.898 for the small cage and 0.782 for the large cage. On the basis of this simple *S* value model, for methane and xenon hydrate, the small cage in sI would be expected to form first as observed.

NMR peak areas represent only those small and large cages that are occupied by the guest molecules. The ^{13}C NMR data in this work could not detect any methane in large cages. The amount of CH_4 in $5^{12}6^4$ was shown to be small relative to the total amount of CH_4 in hydrate by earlier NMR and Raman observations.[13,19] Hence, in the following calculations, the methane large cage occupancy was assumed to be zero.

The NMR data suggested that the ratio of growth rates (large cage to small cage) ranged from 1.45 to 2.57, with one outlier of 22.0 in Table 2, when sII was formed from a $CH_4 + C_3H_8$ gas mixture with 40% methane and 60% propane at 269 K and a pressure ranging between 0.34 and 0.84 MPa. At any given time, the propane-occupied large cages averaged twice that of the methane occupied small cages.

From kinetic data in this work,

$$\frac{\text{number of } 5^{12}6^4 \text{ occupied by } C_3H_8}{\text{number of } 5^{12} \text{ occupied by } CH_4} \approx 2 \qquad (5)$$

Yet, in a sII unit cell,

$$\frac{\text{number of } 5^{12}6^4}{\text{number of } 5^{12}} = \frac{8}{16} = \frac{1}{2} \qquad (6)$$

The number of occupied cages is equal to the total number of cages times the cage occupancy. Assuming C_3H_8 occupancy of large cages is unity, and the CH_4 fractional occupancy of small cages is equal to *y*,

$$\frac{\text{number of } 5^{12}6^4 \text{ occupied by } C_3H_8}{\text{number of } 5^{12} \text{ occupied by } CH_4} = \frac{1}{2} \cdot \frac{1}{y} \qquad (7)$$

From eqs 5 and 7,

$$y = 0.25 \qquad (8)$$

Therefore, the percentage of methane-occupied small cages in sII during initial hydrate growth in our experiments was 25%. Modifying the above analysis to include occupancy of large cages by methane would increase the ratio of eq 7 and decrease the percentage of methane-occupied small cages given by eq 8. Therefore, eqs 7 and 8 provide lower and upper bounds, respectively.

Figure 10 shows the mole fraction of CH_4 as a function of time in the vapor and hydrate phase in the surface reaction regime of hydrate formation. Hydrates were formed with ice particles of diameter ranging from 840 to 1180 μm, at 0.67 MPa and 269 ± 0.5 K. The CH_4 compositions of the vapor and hydrate phase were calculated from NMR peak areas as described by Subramanian et al..[20] The CH_4 and C_3H_8 peak intensities for hydrate cages and vapor were presented in Figure 5.

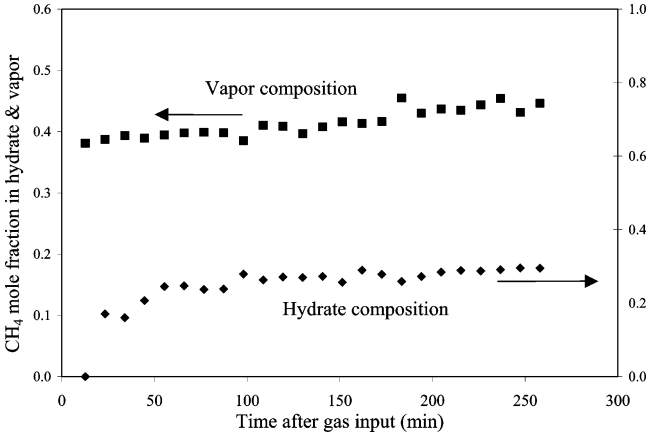

Figure 10. CH_4 mole fraction of hydrate and vapor as a function of time in the surface reaction regime of hydrate formation with ice particle of 840 μm < *D* < 1180 μm at 0.67 MPa and 269 ± 0.5 K.

Figure 4 showed that methane and propane concentrations in vapor and hydrate remained approximately constant in the slow growth regime. Typically, the vapor composition changed during the surface reaction linear growth. However, once the linear growth ended, the vapor and hydrate compositions did not change significantly. The compositions at the end of the linear growth were used in the cage occupancy calculations. The CH_4 mole fraction in hydrate and vapor during the linear growth in one of the experiments are shown in Figure 10.

A state-of-the art in-house hydrate program, CSMGem, developed by Ballard and Sloan,[21] was used to predict small cage occupancy in $CH_4 + C_3H_8$ sII hydrate as a function of equilbrium gas composition. The CSMGem program predicted that a $CH_4 + C_3H_8$ gas mixture with 40% CH_4 and 60% C_3H_8 forms sII hydrate at 0.67 MPa and 269 K. The predicted occupancy of CH_4 in the 5^{12} is 44%, CH_4 in the $5^{12}6^4$ is 0%, and C_3H_8 in the $5^{12}6^4$ is 100%. The propane molecule is too large to fit into the 5^{12} cage of sII. Though our kinetic data showed CH_4 occupancy of the 5^{12} to be about 25% during early hydrate formation, the thermodynamic model suggested the occupancy at the steady state to be 44%. The experimental result that $5^{12}6^4$ cages filled with C_3H_8 formed twice as fast as small cages occupied by CH_4, was attributed to the formation of sII unit cells with only about 25% of 5^{12} cages occupied by CH_4. This suggests that more 5^{12} would become filled over long times as the system comes to equilibrium.

6. Conclusions

The kinetics of $CH_4 + C_3H_8$ sII hydrate formation from ice was measured using conventional ^{13}C NMR spectroscopy. A hydrate formation mechanism hypothesis was partitioned into two regimes: (1) surface reaction controlled and (2) solid diffusion. In the surface reaction-controlled regime, large cages filled with propane formed twice as fast as small cages filled with methane because propane-occupied large cages were more stable and abundant than methane-occupied small cages. Propane preferentially entered the hydrate, denuding the vapor of propane. The slope of a growth curve for the surface reaction was directly proportional to the reaction rate of hydrate formation.

The reaction rate of cage formation and the time to form a complete hydrate layer on the particle surface were linearly proportional to the surface-to-volume ratio of ice particles and to pressure. The cage growth rate increased with the feed partial pressure for a given ice particle size. A hypothesis for the faster growth of large cages was based on $CH_4 + C_3H_8$ sII hydrate formation with only 25% of 5^{12} occupied by CH_4. A simple kinetic model was developed on the basis of the hydrate growth data.

Acknowledgment. We thank Texaco Graduate Foundation for granting a graduate fellowship to R. K. This work was partially funded by a consortium of oil companies, BP, ChevronTexaco, Unocal, Marathon, U.S. DoE, ConocoPhillips, and Petrobras. Authors gratefully recognize the National Research Council (NRC) of Canada, who acted as a mentor institution for R.K. during the period of July 2 to August 16, 1998, to enable his work on hydrates. We thank Professor Carolyn A. Koh of Colorado School of Mines for helpful discussions.

Appendix A: Temperature Change during Hydrate Formation from Ice (Refer to Section 4.2)

Basis: 1 μm thick hydrate layer on the surface of a 500 μm diameter ice particle

Heat of fusion of ice, $\Delta H_{ice} = 333.7$ kJ/kg of ice (endothermic)[22]

Heat of sII hydrate formation = 526.6 kJ/kg of hydrate (exothermic)[23]

Density of ice,[19] ρ_{ice} = density of hydrate, $\rho_{hydrate} = 917$ kg/m^3

Heat capacity of ice, $C_{p,ice} = 2.1$ kJ/(kg·K)[22]

Heat capacity of hydrate, $C_{p,hydrate} = 2.1$ kJ/(kg·K) (assumed to be the same as ice)

ΔT_m (K) = Change in temperature of ice particle

From heat balance,

$$\text{mass of ice particle (of diameter 499 } \mu\text{m)} \times C_{p,ice} \times \Delta T_m + \text{mass of hydrate layer (1 } \mu\text{m thick)} \times C_{p,hydrate} \times \Delta T_m = \text{mass of melted ice (of 1 mm thick layer)} \times \Delta H_{ice} \quad (9)$$

$$\text{volume of ice particle} \times \rho_{ice} \times C_{p,ice} \times \Delta T_m + \text{volume of hydrate layer} \times \rho_{hydrate} \times C_{p,hydrate} \times \Delta T_m = \text{volume of melted ice} \times \rho_{ice} \times \Delta H_{ice} \quad (10)$$

$$\frac{\pi \times 499^3}{6}(\mu\text{m})^3 \times 917\ (\text{kg/m}^3) \times 2.1\ [\text{kJ/(kg·K)}] \times \Delta T_m\ (\text{K}) + \frac{\pi \times (500^3 - 499^3)}{6}(\mu\text{m})^3 \times 917\ (\text{kg/m}^3) \times 2.1[\text{kJ/(kg·K)}] \times \Delta T_m\ (\text{K}) = \frac{\pi \times (500^3 - 499^3)}{6}(\mu\text{m})^3 \times 917\ (\text{kg/m}^3) \times 333.7\ (\text{kJ/kg}) \quad (11)$$

$\Delta T_m = 0.95$ K, the decrease in temperature of ice particle due to endothermic ice melting is 0.95 K.

Similar calculations were done to calculate the change in temperature due to exothermic hydrate formation (ΔT_f), by replacing the heat of ice melting with the heat of hydrate formation. Because the heat of hydrate formation is about 1.6 times the heat of fusion of ice, the temperature increase due to hydrate formation (ΔT_f) is approximately 1.5 K.

Supporting Information Available: Figure 1S shows the ratio of peak intensities for C_3H_8 in 5^12^64 to CH_4 in 5^{12} as a function of time in the linear growth regime. The peak intensities were obtained from the linear fit to the data shown in Figures 4 and 5. This material is available free of charge via the Internet at http://pubs.acs.org.

References and Notes

(1) Katz, D. L.; Cornell, D.; Vary, J. A.; Kobayashi, R.; Elenbaas, J. R.; Poettmann, F. H.; Weinaug, C. F. *Handbook of Natural Gas Engineering*; McGraw-Hill Book Company, Inc.: New York, 1959.

(2) Sloan, E. D., Jr. *Clathrate Hydrates of Natural Gases*, 2nd ed.; Marcel Dekker Inc.: New York, 1998; 705 pp and software included.

(3) Englezos, P.; Kalogerakis, N.; Dholabhai, P. D.; Bishnoi, P. R. *Chem. Eng. Sci.* **1987**, *42*, 11, 2647. Englezos, P.; Kalogerakis, N.; Dholabhai, P. D.; Bishnoi, P. R. *Chem. Eng. Sci.* **1987**, *42*, 11, 2659;.Englezos, P.; Bishnoi, P. R. *Fluid Phase Equilib.* **1988**, *42*, 129. Skovborg, P. Gas Hydrate Kinetics. Ph.D. Thesis, Institute fir Kemiteknik, Denmark, 1993. Skovborg, P.; Rasmussen, P. *Chem. Eng. Sci.* **1994**, *49*, 8, 1131. Christiansen, R. L.; Sloan. E. D. *Proc. Annu. GPA Conf., 74th* **1995**, 14.

(4) Barrer, R.; Edge, A. V. J. *Proc. R. Soc. (London)*. **1967**, A300. Miller, S. L.; Smythe W. D. *Science* **1970**, *170*, 531. Falabella, B. J. A Study of Natural Gas Hydrates. Ph.D. Thesis, University of Massachusetts, 1975. Kamath V. A. Study of Heat Transfer Characteristics during Dissociation of Gas Hydrates. Ph.D. Thesis, University of Pittsburgh, 1984. Hwang, M. J.; Wright, D. A.; Holder, G. D. *J. Inclusion Phenom.* **1990**, *8* (1, 2), 103.

(5) Englezos, P. *Proc. Fifth Int. Offshore Polar Eng. Conf.*. **1995**, 289.

(6) Pietrass, T.; Gaede, H. C.; Bifone, A.; Pines, A.; Ripmeester, J. A. *J. Am. Chem. Soc.* **1995**, *117*, 7520.

(7) Moudrakovski, I. L.; Sanchez, A. A.; Ratcliffe, C. I.; Ripmeester, J. A. *J. Phys. Chem. B* **2001**, *105*, 12338.

(8) Fleyfel, F.; Song, K. Y.; Kook, A.; Martin, R.; Kobayashi, R. *Proc. Int. Conf. Natural Gas Hydrates* **1994**, 212.

(9) Subramanian, S. Measurements of Clathrate Hydrates Containing Methane and Ethane Using Raman Spectroscopy. Ph.D. Thesis, Colorado School of Mines, Golden, CO, 2000.

(10) Wang, X.; Schultz, A. J.; Halpern, Y. *Proc. Fourth Int. Conf. Gas Hydrates* **2002**, 455.

(11) Earl, W. L.; VanderHart, D. L. *J. Magn. Reson.* **1982**, *48*, 35.

(12) Van Geet, A. L. *Anal. Chem.* **1970**, *42*, 679.

(13) Ripmeester, J. A.; Ratcliffe, C. I. *J. Phys. Chem.* **1988**, 92, 337.

(14) Uchida, T.; Moriwaki, M.; Takeya, S.; Ikeda, I. Y.; Ebinuma, T.; Nagao, J.; Narita, H.; Gohara, K.; Mae, S. *Proc. Fourth Int. Conf. Gas Hydrates* **2002**, 553.

(15) Gardiner, W. C., Jr. *Rates and Mechanisms of Chemical Reactions*; Benjamin: Reading, MA, 1969.

(16) Moore, W. J. *Physical Chemistry*, 4th ed.; Prentice-Hall: Englewood Cliffs, NJ, 1972; 325 pp.

(17) Christiansen, R. L.; Sloan, E. D. *Proc. Int. Conf. Natural Gas Hydrates* **1994**, 283.

(18) Seth, B. B. L.; Ross, H. U. *Trans. Metall. Soc. AIME* **1965**, Vol. 233, 180.

(19) Sum, A. K.; Burruss, R. C.; Sloan, E. D. *J. Phys. Chem. B* **1997**, *101*, 7371.

(20) Subramanian, S.; Ballard, A. L.; Kini, R. A.; Dec, S. F.; Sloan, E. D., Jr. *Chem. Eng. Sci.* **2000**, *55*, 5763.

(21) Ballard, A. L.; Sloan, E. D., Jr. *Fluid Phase Equilib.* **2002**, *371*, 194.

(22) *CRC Handbook of Chemistry and Physics*, 66th ed.; CRC Press: Boca Raton, FL, 1986.

(23) Kelkar, S. K.; Selim, M. S.; Sloan, E. D., Jr. *Fluid Phase Equilib.* **1998**, *371*, 150.